

Article

NDVI Threshold-Based Urban Green Space Mapping from Sentinel-2A at the Local Governmental Area (LGA) Level of Victoria, Australia

Jagannath Aryal ^{1,*}, Chiranjibi Sitaula ² and Sunil Aryal ³

¹ Faculty of Engineering and IT, The University of Melbourne, Parkville, VIC 3010, Australia

² Department of Electrical and Computer Systems Engineering, Monash University, Melbourne, VIC 3800, Australia; Chiranjibi.Sitaula@monash.edu

³ School of Information Technology, Deakin University, Waurn Ponds, VIC 3216, Australia; sunil.aryal@deakin.edu.au

* Correspondence: jagannath.aryal@unimelb.edu.au

Abstract: Obtaining accurate, precise and timely spatial information on the distribution and dynamics of urban green space is crucial in understanding livability of the cities and urban dwellers. Inspired from the importance of spatial information in planning urban lives, and availability of state-of-the-art remote sensing data and technologies in open access forms, in this work, we develop a simple three-level hierarchical mapping of urban green space with multiple usability to various stakeholders. We utilize the established Normalized Difference Vegetation Index (NDVI) threshold on Sentinel-2A Earth Observation image data to classify the urban vegetation of each Victorian Local Government Area (LGA). Firstly, we categorize each LGA region into two broad classes as vegetation and non-vegetation; secondly, we further categorize the vegetation regions of each LGA into two subclasses as shrub (including grassland) and trees; thirdly, for both shrub and trees classes, we further classify them as stressed and healthy. We not only map the urban vegetation in hierarchy but also develop Urban Green Space Index (UGSI) and Per Capita Green Space (PCGS) for the Victorian Local Government Areas (LGAs) to provide insights on the association of demography with urban green infrastructure using urban spatial analytics. To show the efficacy of the applied method, we evaluate our results using a Google Earth Engine (GEE) platform across different NDVI threshold ranges. The evaluation result shows that our method produces excellent performance metrics such as mean precision, recall, f-score and accuracy. In addition to this, we also prepare a recent Sentinel-2A dataset and derived products of urban green space coverage of the Victorian LGAs that are useful for multiple stakeholders ranging from bushfire modellers to biodiversity conservationists in contributing to sustainable and resilient urban lives.



Citation: Aryal, J.; Sitaula, C.; Aryal, S. NDVI Threshold-Based Urban Green Space Mapping from Sentinel-2A at the Local Governmental Area (LGA) Level of Victoria, Australia. *Land* **2022**, *11*, 351. <https://doi.org/10.3390/land11030351>

Academic Editor: Le Yu

Received: 28 January 2022

Accepted: 24 February 2022

Published: 27 February 2022

Publisher's Note: MDPI stays neutral with regard to jurisdictional claims in published maps and institutional affiliations.



Copyright: © 2022 by the authors. Licensee MDPI, Basel, Switzerland. This article is an open access article distributed under the terms and conditions of the Creative Commons Attribution (CC BY) license (<https://creativecommons.org/licenses/by/4.0/>).

1. Introduction

Remote sensing images are widely used to study and analyze the landscapes such as vegetation cover, which covers around 70% of the earth surface [1]. The remote sensing images are available from several dedicated sources, platforms and repositories, such as NASA, ESA, Google Earth [2], Copernicus Open Access Hub [3], EO Browser [4], United States Geological Survey (USGS) [5], and so on. Among them, Copernicus Open Access Hub is one of the popular open-source repositories to access Sentinel-2A product in analyzing vegetation. The urban vegetation/green space analysis is very important to achieve the goals of sustainable urbanization [6]. It is recognized that vegetation information provides adaptable resources for handling (controlling and moderating) the varieties of problems on the urbanization issues [7]. Furthermore, the biophysical processes of urbanization are

influenced by the spatial distribution of urban green space [8]. Urban vegetation can be considered as a foundation element of greenprinting, which is the process of developing a conservation strategy. Greenprinting documents the environmental, economic and social benefits that trees, parks, and other types of green space provide to urban communities and urban dwellers.

Furthermore, the urban vegetation information can be an invaluable resource in land use and land cover (LULC) classification. Vegetation information can be extracted using a spectral signature, which is the graphical representation showing the relationship between wavelengths and reflectance values in a different spectrum. Urban spatial analytics is an emerging analytical capability to leverage data science in addressing major issues cities continue to face. Issues and processes on air filtration, water run off, land pollution, carbon emissions and eventually liveability are directly related to the density and abundance of urban green space.

A Normalized Difference Vegetation Index (NDVI) is a very important and simple measure that has been used in the literature for the land use land cover (LULC) classification in varieties of landscapes [9–11]. Ghaderpour et al. [9] highlighted that NDVI changes with the surface temperature in a Tunisian context. Furthermore, Abdullah et al. [10] carried out the study of spatio-temporal pattern changes in Bangladesh, which utilized NDVI for the training data generation. Similarly, Kwan et al. [11] carried out the vegetation and non-vegetation classification using a machine learning classifier, called Support Vector Machine (SVM), in reporting the efficacy of NDVI values for the classification. These works, overall, highlight the applications of NDVI for land cover classification and changes via urbanization, deforestation, drought, etc. However, previous works in the literature [12–32] for LULC classification reveal that there are no universal methods and tools that work equally well in LULC classification for all countries and regions on the earth. That is, the analysis of such images is landscape-specific. This is because of the geographical variability of the real world in space and time. In such a case, we need to develop models for transferability where possible by capturing geographical elements such as topography, density, abundance and phenology of vegetation of local territories and importantly develop workflows.

Multi-level hierarchical LULC classification helps understand the categorization of different urban green regions. Thus, our goal is to classify vegetation regions into finer level of categories from the lens of application such that the derived data and products can work as a basis for further research applications in environmental sustainability and infrastructure design. In this work, we use the NDVI for LULC classification at three levels to identify different urban vegetation regions. We used this technique to analyse the distribution of vegetation at the Local Government Area (LGA)-level of the state of Victoria in Australia. We first create a database of remote sensing images (Sentinel-2A) for each LGA¹. In doing this, firstly, we accessed and collected the images from the open-source repository. Secondly, to identify and classify different regions in the remote sensing images, we utilise the specific NDVI threshold ranges at three different levels of classification hierarchy for the study area. We further develop the relationship of vegetation abundance and their association with demography. We compute Urban Green Space Index (*UGSI*) and Per Capita Green Space (*PCGS*) for all Local Government Areas (LGAs). This index-based information will contribute to further developing policy insights in the domain of sustainability and resilience research agendas of the cities.

The main contributions of this paper are as follows:

1. Utilisation of high quality and publicly available low cost remote sensing data for mapping and monitoring of urban green vegetation abundance.
2. Utilisation of mainstream image visualisation platform Google Earth Engine (GEE) [2] and open source GIS software—QGIS [33] for hierarchical mapping of urban vegetation.
3. Evaluation and selection of NDVI threshold ranges using a quantitative iterative optimal approach.
4. Development of indices and insights on the association of demography with urban green infrastructure.

The paper is organized as follows. In Section 2, we discuss related works followed by study materials (the study area, data sets used, NDVI utilization, Urban Green Space and Per Capita Green Space conceptualisation) used in Section 3. Similarly, in Section 4, we discuss our proposed method in a step-wise manner. Section 5 presents the results and discussion. Finally, in Section 6, we conclude our work with the recommended future works.

2. Related Works

Application of remote sensing research utilizing multi-sensor, multi-resolution and multiple platform satellite images such as Landsat-8, Sentinel-2A/2B products, Moderate Resolution Imaging Spectroradiometer (MODIS), LiDAR (Light Detection and Ranging), Unmanned Aerial Vehicle (UAV) images, etc. contributed significantly for the land use and land cover (LULC) classification. To capture the breadth of LULC classification methods, within the scope of NDVI, these are grouped into two broad categories: Section 2.1 index-based classification and Section 2.2 machine learning-based classification.

2.1. Index-Based Classification

In index-based classification [12–15], classification is performed using a threshold of NDVI value for each pixel in the image. For instance, Montandon et al. [12] utilized an NDVI threshold for the LULC classification. They also performed change detection for different regions. Furthermore, Sahebjalal et al. [13] used an NDVI value to perform the change detection using Landsat images. Similarly, Gascon et al. [14] used NDVI value as a marker of surrounding of plants for the epidemiological studies in Spain. Furthermore, recently Da Silva et al. [15] utilized five vegetation indices, including NDVI to classify the land covers in Brazil.

2.2. Machine Learning-Based Classification

In machine learning-based methods [16–30], classification is performed by using two approaches: unsupervised and supervised approach. In the unsupervised approach, class labels are not provided and classification is performed using pattern recognition on the fly, whereas, in the supervised approach, pre-defined class labels are provided. Furthermore, machine learning-based methods can be broadly subdivided into two categories: Section 2.2.1 traditional machine learning-based methods and Section 2.2.2 deep learning-based methods.

2.2.1. Traditional Machine Learning-Based Classification

Traditional machine learning-based methods [16–22,31,32] are basically based on popular algorithms, such as Random Forest (RF) [34], Support Vector Machine (SVM) [35], Maximum Likelihood Algorithm (MLA) [36], etc., whereas recent deep learning-based methods use recent advances of deep learning models, such as Convolution Neural Networks (CNNs), Auto Encoders (AEs), etc. For example, Kocev et al. [31] employed an ensemble of decision trees to perform land cover classification of Victoria, Australia. Their method used Landsat 7 images in the experiment. Sheffield et al. [32] adopted C4.5 and C5.0 algorithms on the MODIS dataset to classify the land use and land cover of Victoria, Australia. Similarly, Zhang et al. [20] evaluated different bands of Sentinel-2A image and compared index-based classification with the SVM algorithm for the classification of different regions in such images into four categories (crop, tree, water, and road). Liu et al. [21] employed Sentinel-1A, Topographic Mission Digital Elevation (DEM), Landsat-8, and Sentinel-2A image for the forest type identification using an RF algorithm. Mensah et al. [16] applied four different kinds of remote sensing images (Landsat-4, Landsat-7, Sentinel-2A, and Worldview-3) and classified using MLA for the change detection in Ghana. Similarly, Daryaei et al. [17] utilized an RF algorithm for fine-scale detection of vegetation on UAV images and Sentinel-2A images. Abutaleb et al. [18] also used an RF algorithm in addition to NDVI value to identify the affluent and poor suburb of Johannesburg. Cai et al. [19]

utilized mixture models, such as fully constrained least squares (FCLS), SVM, and k-nearest neighborhood (KNN) for the urban fractional vegetation cover using Sentinel-2A images. Vasilakos et al. [22] combined the results of multiple machine learning algorithms (Decision Tree, Discriminant, SVM, KNN, RF, Artificial Neural Network (ANN)) using voting methods on multi-temporal Sentinel-2A datasets for the LULC classification. Recent research [37] also shows that SVM outperforms other popular algorithms, such as RF, XGBoost [38], etc. in LULC classification.

2.2.2. Deep Learning-Based Classification

Recently, researchers used several state-of-the-art (SOTA) deep learning models [24–30]. Ghorbanzadeh et al. [24] applied CNN models in addition to other traditional machine learning methods for landslide mapping and evaluated the applied methods using various quantitative metrics. From their works, it is recommended that CNN is still in its infancy, yet it has immense potential if we can perform proper data augmentation and architecture tuning. Timilsina et al. [25] adopted CNNs for urban tree cover changes in Tasmania, Australia using the LiDAR dataset. Li et al. [26] employed a Stacked Autoencoder (SAE) for remote sensing image classification. Their result shows that SAE outperforms other algorithms, such as RF, SVM, and ANN. Similarly, Liang et al. [27] also used Stacked Denoising Auto Encoder (SDAE) for remote sensing image classification, which has shown that SDAE outperforms SVM and ANN. Tong et al. [28] exploited a pre-trained CNN model (ResNet-50 [39]) for the land cover classification using different types of remote sensing images, such as Gaofen-2, Gaofen-1, Jilin-1, Ziyuan-3, Sentinel-2A, and Google Earth platform data. Brahme et al. [29] employed pre-trained deep learning models (VGG-Net [40] and Inception-V3 [41]) to extract the built-up areas from Sentinel-2A images. Luo et al. [30] proposed a hybrid convolution neural network (H-ConvNet) to improve the performance of urban land cover mapping using Sentinel-2A images.

The above section on related works (Section 2) showcases the breadth and importance of urban green space mapping utilising evolving computational technologies. However, a simple and powerful application is needed for the replicability and understanding of the mapping of basic foundational spatial layers of urban green space that are useable in the local setting by the decision makers in planning the cities. Therefore, these maps/data sets can be used as a basis for other research and decision support systems without having difficulties in the replication of the work.

3. Materials

3.1. Study Area

All local government areas (LGAs) except Bass Coast Shire of Victoria, Australia, were considered in our study. We accessed publicly available polygons data in GeoJSON file format from the Victorian government's website [42]. The location of our study area (Victorian LGAs) is presented in Figure 1. Victoria has several native vegetation types, including Tall Greenhood (*Pterostylis melagramma*), Common Plait-moss (*Hypnum cupressiforme*), Slender Dodder-laurel (*Cassytha glabella*), Lysiana exocarpi (*Harlequin Mistletoe*), etc. [43]. This native vegetation is characterized by seven broad factors: (i) diversity of species, (ii) structural complexity, (iii) ages, (iv) fallen timber, lichen, etc. (v) fungi and others, (vi) weeds, and (vii) associations with other vegetation [44]. Victoria has mostly pleasant temperatures except some hot days in summer. In summer, the average maximum temperature lies in between 40 to 43 degrees, whereas the average minimum temperature lies in between 9 to 15 degrees. In winter, the average maximum temperature lies in between 13 to 16 degrees, whereas the average minimum temperature lies below 10 degrees. Overall, the climate of Victoria is generally favourable to plant growth because of the balance of adequate rainfall and warmth in most parts of the LGAs [45].

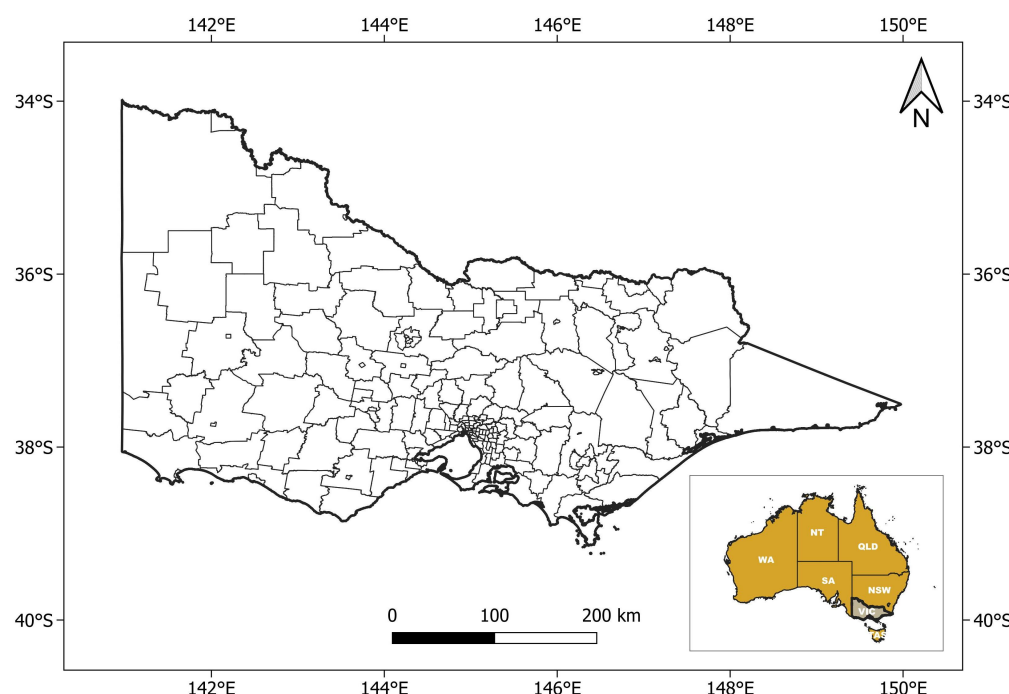


Figure 1. Victorian LGAs mapped in World Geodetic System (WGS) 84 coordinate reference system. These individual LGAs are used in mapping urban green space abundance, developing Urban Green Space Index (*UGSI*) and Per Capita Green Space (*PCGS*) employing demographic data.

3.2. Satellite Images: *Sentinel-2A*

In developing the experimental design, we used *Sentinel-2A* satellite images for each LGA, which were secured from the Copernicus Open Access Hub [3]. The *Sentinel Level-2A* products were radiometrically, atmospherically, and geometrically corrected, which provides the Bottom Of Atmosphere (BOA) reflectance under Universal Transverse Mercator (UTM)/WGS84 projection [46–48]. *Sentinel-2A* comes with three spatial resolutions, including 10 m, 20 m, and 60 m, with 13 spectral bands in total [49]. We derived the surface reflectance value from the *Sentinel-2A* BOA product. The detail description of *Sentinel-2A* product is presented in Table 1.

Table 1. Description of *Sentinel-2A* satellite image providing band details, corresponding Central Wavelength in (nm) and Spatial Resolution (m) in three columns, respectively.

| Band | CW (nm) | SR (m) |
|--|---------|--------|
| Band 1—Coastal aerosol | 443 | 60 |
| Band 2—Blue | 490 | 10 |
| Band 3—Green | 560 | 10 |
| Band 4—Red | 665 | 10 |
| Band 5—Vegetation red edge | 705 | 20 |
| Band 6—Vegetation red edge | 740 | 20 |
| Band 7—Vegetation red edge | 783 | 20 |
| Band 8—Near infrared (NIR) | 842 | 10 |
| Band 8A—Narrow near infrared (NIR) | 865 | 20 |
| Band 9—Water vapour | 945 | 60 |
| Band 10—Shortwave infrared (SWIR)-Cirrus | 1375 | 60 |
| Band 11—Shortwave infrared (SWIR) | 1610 | 20 |
| Band 12—Shortwave infrared (SWIR) | 2190 | 20 |

3.3. Normalized Difference Vegetation Index

The normalized difference vegetation index (NDVI) [50] is one of the popular indicators of vegetation presence in the landscape. The range of NDVI index lies between -1 and $+1$. A higher NDVI index value indicates a higher concentration of vegetation on the ground. Generally, the negative NDVI index value indicates non-green regions such as: barren, sea, river and built-up, whereas the positive value represents green regions [10]. In addition, the NDVI value can be used to identify the health of the plants/vegetation communities. This is because of the fact that healthy plants/vegetation communities are expected to have a higher NDVI values than unhealthy plants.

The NDVI is calculated as in Equation (1):

$$\text{NDVI} = \frac{\text{NIR [Band 8]} - \text{RED [Band 4]}}{\text{NIR [Band 8]} + \text{RED [Band 4]}} \quad (1)$$

where NIR [Band 8] and RED [Band 4] represent the near-infrared and the red band of Sentinel-2A image product, respectively. We present the sample NDVI map for different regions of the City of Melbourne in Figure 2.

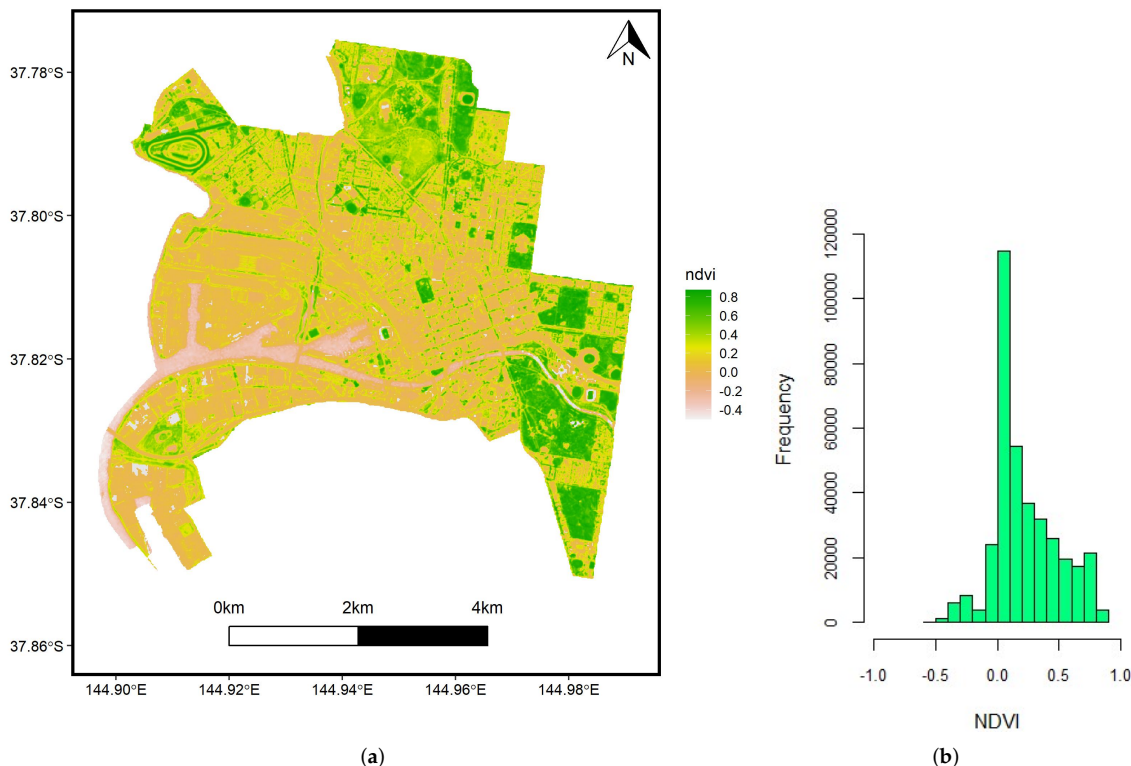


Figure 2. The NDVI map (a) and histogram of NDVI values showing their distribution (b) of City of Melbourne, Victoria, Australia.

3.4. Urban Green Space Index and per Capita Green Space

Urban Green Space Index (*UGSI*) [51] is adopted to calculate the urban green space in the particular area. Furthermore, this identifies the amount of green space in the particular regions of study. Mathematically, it is shown in Equation (2):

$$UGSI_i = \frac{G_i}{A_i}, \quad (2)$$

where $UGSI_i$, G_i and A_i denote *UGSI* of i th unit, green space area in i th spatial unit, and the area of i th unit, respectively. For the calculation of *UGSI* for each LGA, we utilize

three sub-vegetation regions: low vegetation, medium vegetation, and high vegetation. In addition, note that we mention *UGSI* of the non-vegetation region as None in our work.

Furthermore, Per Capita Green Space (*PCGS*) [51] provides the average allocation of green space per person in a particular region (refer to Equation (3)):

$$PCGS_i = \frac{G_i}{PN_i}, \quad (3)$$

where $PCGS_i$, G_i , and PN_i denote *PCGS* in i , green space in i , and population of i , respectively. To calculate *PCGS* in our work for each LGA, we consider total green space area (G_i) and total population (PN_i) of the corresponding LGA. Note that the population of each LGA we used in this work is for the year of 2019, which is the latest information available in the Australian Bureau of Statistics [52].

4. Methods

Our proposed method comprises the following steps: Section 4.1 Acquisition and pre-processing of Sentinel-2A images, Section 4.2 Level-1 classification, Section 4.3 Level-2 classification, and Section 4.4 Level-3 classification. Finally, Section 4.5 Accuracy assessment is used to evaluate our method. Detailed workflow of our work is presented in Figure 3.

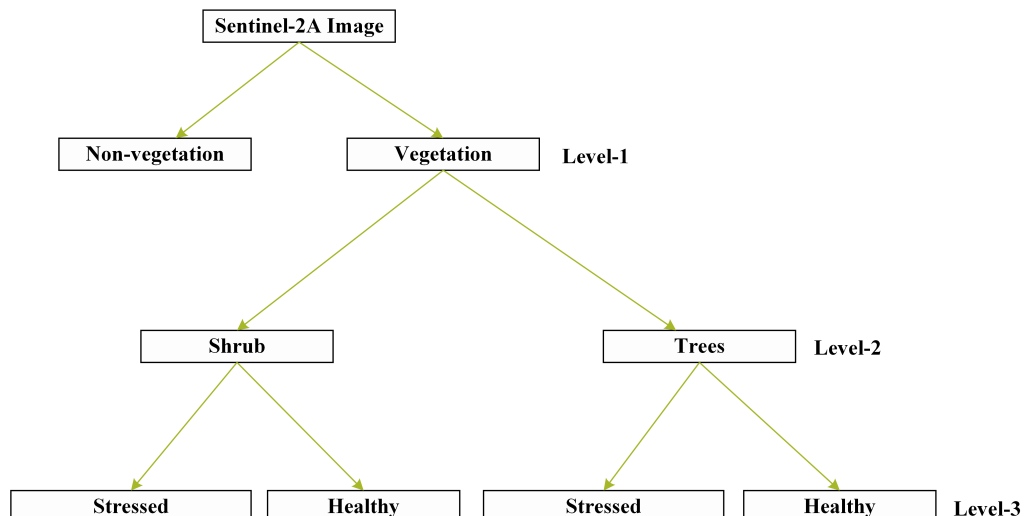


Figure 3. High level workflow of our method, which shows the hierarchical classification at three levels (Level-1, Level-2, Level-3) based on hard NDVI threshold ranges. Note that, in Level-1, we differentiate regions into Non-vegetation and Vegetation regions. Similarly, in Level-2, we differentiate regions into Shrub and Trees regions. Finally, in Level-3, both Shrub and Trees regions are differentiated into Stressed and Healthy regions each.

4.1. Acquisition and Pre-Processing of the Sentinel-2A Dataset

First, we download the Sentinel-2A dataset from the Copernicus Open Access Hub on the fly using a GeoJSON file [42]. However, cloud coverage is one of the hurdles we face during the acquisition of the satellite images. For this, we limit the cloud coverage range from 0 to 10 in our experiment. Meanwhile, we utilize a specific time range (14 November 2019 to 14 April 2020) to find a pristine day for cloud-free or lesser cloudy satellite images. To download the images for the given range, we wrote our code in R language [53] using the Sen2r package [54]. Similarly, for additional pre-processing during accuracy assessment, we adopt the Google Earth Engine (GEE) and QGIS, which are open source software platforms widely used in the remote sensing and spatial analysis domain.

We present RGB (Red, Green, and Blue) true color and false-color (NIR, Red, and Green) Sentinel-2A image of City of Melbourne in Figure 4. For RGB true colour images, we stack three different bands (band 4 for Red, band 3 for Green, and band 2 for Blue) and,

for false colour, we replace Red with an NIR spectral band (Band 8) in addition to Green and Blue colours. False-colour images display more vegetation information by using the NIR band, which is one of two components for the calculation of NDVI value. Note that each image used in our experiment is formed by combining the required spectral bands such as R, G, B, etc. from the bottom-of-the-atmosphere (BOA) of the acquired dataset.

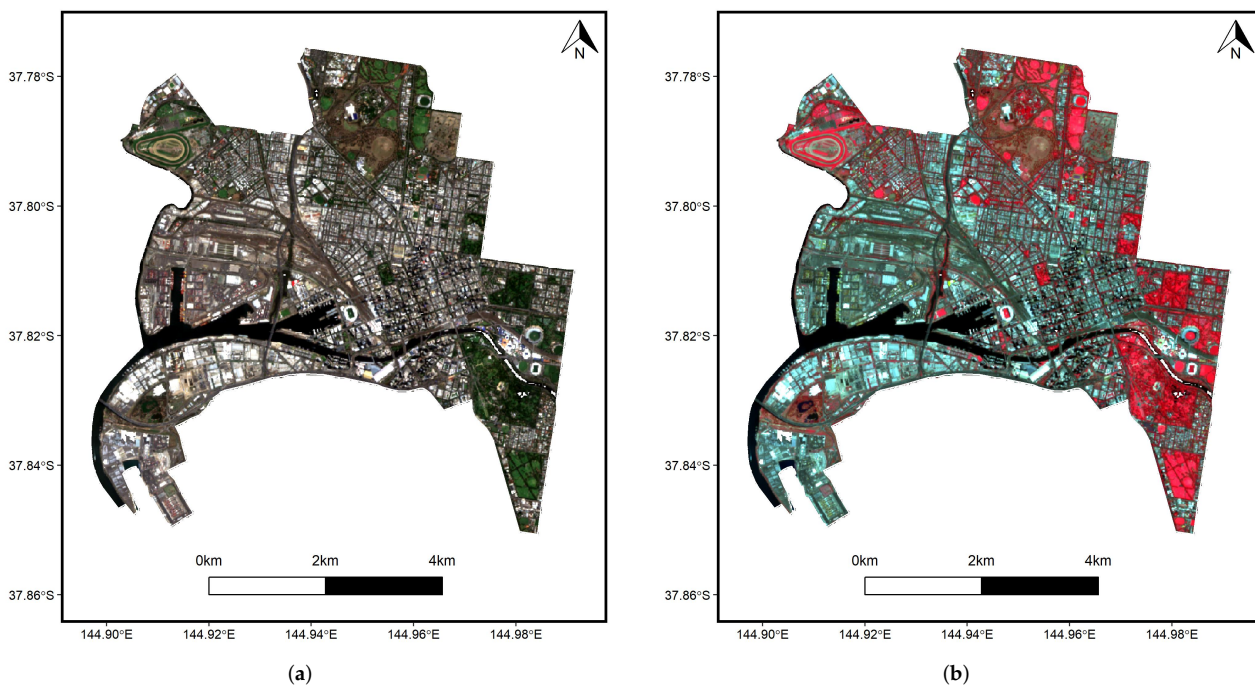


Figure 4. Red Green Blue (RGB) Sentinel-2A image (**a**) and False Colour Sentinel-2A image (**b**) of the City of Melbourne, Victoria, Australia.

4.2. Level-1 Classification

Second, we categorize the target image into vegetation (such as trees, bushes, etc.) and non-vegetation (such as built up, water, etc.) categories for each LGA. For this, we utilize the hard threshold of NDVI values as suggested by the previous studies and methods [1,12,55,56]. To this end, by using the NDVI threshold value on each pixel in the target image, we segment the corresponding image into the two broad regions. As an example, we have presented the Level-1 classification of the City of Melbourne, Victoria, in Figure 5. In the figure, the non-vegetation such as built up, and water have NDVI value less than 0.19, whereas the vegetation region containing green cover such as ground, bush, trees, etc. have a higher than 0.19 NDVI value (refer to Table 2). We set those values based on an empirical study using a GEE platform.

Table 2. Level-1 classification of LGA into two broad regions: non-vegetation and vegetation.

| Category | Threshold |
|----------------|---------------|
| Vegetation | 0.19 to 1.00 |
| Non-vegetation | −1.00 to 0.19 |

4.3. Level-2 Classification

Third, we further categorize the vegetation region into two sub classes: shrub (including grassland) and trees class coverage. The sample visual output of Level-2 classification is presented in Figure 5. As Level-2 classification, both regions are also segmented using a hard threshold of NDVI value (see details in Table 3).

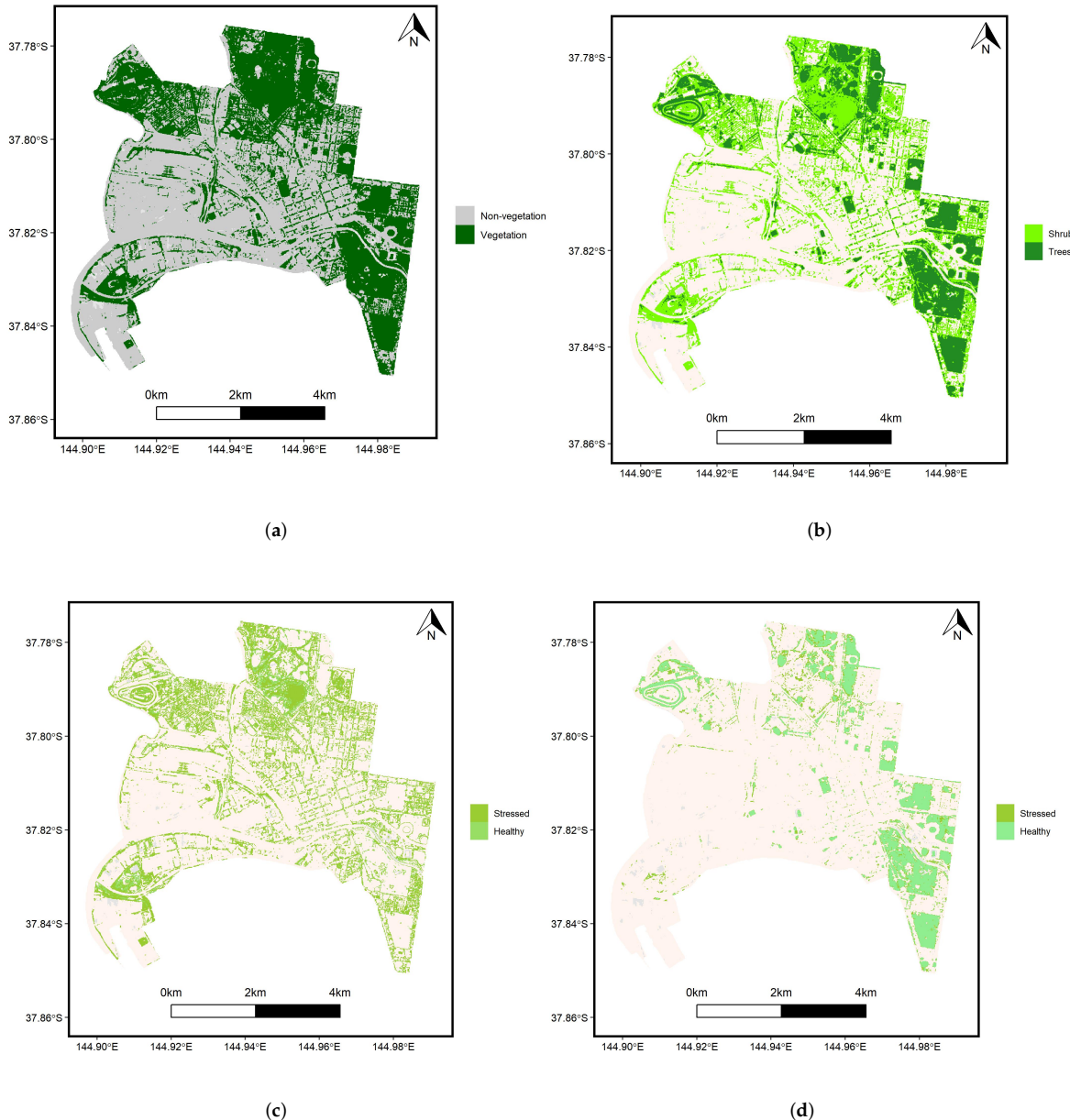


Figure 5. Three different classification levels for City of Melbourne ((a) Level-1 classification, (b) Level-2 classification, (c) Level-3a classification, and (d) Level-3b classification). Note that level-3 contains two classifications level-3a and level-3b for shrub and trees, respectively.

Table 3. Level-2 classification of vegetation region into shrub and trees regions.

| Category | Threshold |
|----------|---------------|
| Shrub | 0.19 to 0.50 |
| Trees | 0.50 to +1.00 |

4.4. Level-3 Classification

Fourth, we further divide regions extracted from Level-2 classification (shrub and trees) into two sub-groups, namely stressed and healthy. The sample output of such classification result is presented in Figure 5. Compared to healthy vegetation, stressed vegetation is expected to have a lower NDVI value. We apply this idea on both shrub

(Level-3a classification) and trees (Level-3b classification) class categories (see details in Tables 4 and 5).

Table 4. Level-3a classification of shrub region into stressed and healthy regions.

| Category | Threshold |
|----------|--------------|
| Healthy | 0.40 to 0.50 |
| Stressed | 0.19 to 0.40 |

Table 5. Level-3b classification of trees region into stressed and healthy regions.

| Category | Threshold |
|----------|---------------|
| Healthy | 0.60 to +1.00 |
| Stressed | 0.50 to 0.60 |

4.5. Accuracy Assessment

To assess the accuracy, we use Google Earth Engine (GEE) [2] and QGIS [33]. First, we identify the random ground truth points of the corresponding LGA using GEE and then set markers based on them using visual inspection. Here, for each level of classification, we randomly select 30 control points (e.g., 30 for vegetation and 30 for non-vegetation at level-1) using human judgement at each level of the classification for four LGAs (see Table 6) used in this study. Then, we tally such markers with our result using QGIS software. This task results in a confusion matrix at each level. Based on such a confusion matrix, we calculate precision (Equation (4)), recall (Equation (5)), f-score (Equation (6)), and accuracy (Equation (7)) for each level. Note that we use four LGAs for the accuracy assessment (refer to Table 6 for the details of such LGAs). Note the accuracy assessment results in each table are the averaged values over four LGAs used in this study:

$$\text{Precision} = \frac{TP}{TP + FP}, \quad (4)$$

$$\text{Recall} = \frac{TP}{TP + FN}, \quad (5)$$

$$\text{F-score} = 2 \times \frac{\text{Recall} \times \text{Precision}}{\text{Recall} + \text{Precision}}, \quad (6)$$

$$\text{Accuracy} = \frac{TN + TP}{TN + TP + FN + FP}, \quad (7)$$

where TP , TN , FP , and FN denotes true positive, true negative, false positive, and false negative, respectively.

Table 6. Details of LGAs used in ablative study of thresholds.

| LGA | Area Approx. (sq. kms.) | Type |
|--------------|-------------------------|--------------|
| Melbourne | 36.90 | Metropolitan |
| Port Phillip | 19.90 | Metropolitan |
| Yarra | 19.30 | Metropolitan |
| Swan Hill | 6095.10 | Rural |

5. Results and Discussion

We present the results obtained for different LGAs of Victoria, discuss the involved processes in achieving the results, provide the insights from the results and contrast them with the previous related works from the literature.

5.1. Results on Various NDVI Threshold Ranges

We analyze different threshold ranges to classify the regions of LGAs at three different levels. We choose four different LGAs, including three LGAs in Melbourne metropolitan area and one rural LGA. This includes LGAs from both rural and metro regions of Victoria. While selecting the candidate LGAs for the ablative study of thresholds, we include both LGAs with higher vegetation regions than non-vegetation regions (City of Port Phillip and City of Yarra) and LGAs with lower vegetation regions than non-vegetation regions (City of Melbourne and Rural City of Swan Hill). Further details of such candidate LGAs used in the ablative study are enlisted in Table 6. To perform this ablative study, for each of four LGAs at each level, we randomly extracted 30 ground truth pixels from the GEE platform and constructed the confusion metrics by comparing such ground truth pixels with our results based on different threshold ranges. To ascertain the optimal range, we have tested our experiment with four different threshold ranges. This provided us confidence on the map production process and robustness in its validation. Out of the four threshold ranges, we used the fourth threshold range to produce and validate the maps in different levels. These results are provided in supplementary File S1. Based on the confusion metrics for all of four LGAs, we calculate and tabulate the mean precision, recall, f-score, and accuracy in the corresponding table of each level. The boldface indicates the best result in the tables. We enlist the results of different threshold ranges used in our method in four different tables: Table 7 for Level-1 classification, Table 8 for Level-2 classification, Table 9 for Level-3a classification, and Table 10 for Level-3b classification. Furthermore, we incorporate Level-3a classification and Level-3b classification under Level-3 classification for shrub and trees, respectively.

Table 7. Accuracy assessment for different threshold ranges at Level-1 classification for vegetation and non-vegetation regions. Note that each row represents the averaged metrics (Precision, Recall, F-score, and Accuracy) of four LGAs under Level-1 classification. The boldface represents the optimal threshold range and resulting best values.

| Non-Vegetation | Vegetation | Precision | Recall | F-Score | Acc. |
|-------------------|------------------|-------------|-------------|-------------|-------------|
| -1 to 0.19 | 0.19 to 1 | 1.00 | 1.00 | 1.00 | 1.00 |
| -1.00 to 0 | 0 to 1.00 | 1.00 | 0.67 | 0.75 | 0.70 |
| -1.00 to 0.20 | 0.20 to 1.00 | 0.95 | 1.00 | 0.95 | 0.97 |
| -1.00 to 0.30 | 0.30 to 1.00 | 0.87 | 1.00 | 0.90 | 0.90 |

Table 8. Accuracy assessment using different threshold ranges at level-2 classification for shrub and trees regions. Note that each row represents the averaged metrics (Precision, Recall, F-score, and Accuracy) of four LGAs under Level-2 classification. The boldface represents the optimal threshold range and resulting best values.

| Shrub | Trees | Precision | Recall | F-Score | Acc. |
|---------------------|---------------------|-------------|-------------|-------------|-------------|
| 0.19 to 0.20 | 0.20 to 1.00 | 0.05 | 0.35 | 0.05 | 0.52 |
| 0.19 to 0.30 | 0.30 to 1.00 | 0.35 | 0.87 | 0.30 | 0.57 |
| 0.19 to 0.40 | 0.40 to 1.00 | 0.55 | 0.90 | 0.55 | 0.67 |
| 0.19 to 0.50 | 0.50 to 1.00 | 0.75 | 0.90 | 0.72 | 0.77 |

5.2. Result of Classified Outputs

We present the consolidated results containing the occupied areas of four different LGAs achieved at three different classification levels. Note that our results are based on 10×10 square meter-sized pixels on the Sentinel-2A satellite images. The results are presented in Figure 6. Four LGAs of inner Melbourne namely City of Melbourne, City of Port Phillip, City of Stonnington and City of Yarra are presented in the form of a chord diagram to showcase the 3-level of urban green classification. We also present four sub-

green regions (non-green, low, middle, and high vegetation) percentages and corresponding per capita green space indexes under vegetation region of all 78 LGAs in three Tables 11–13. Since we present only four LGAs for classification for readability in the paper, we include additional detailed results of remaining LGAs in the supplementary Figure S2.

Table 9. Accuracy assessment using different threshold ranges at Level-3a classification for stressed and healthy regions. Note that each row represents the averaged metrics (Precision, Recall, F-score, and Accuracy) of four LGAs under Level-3a classification. The boldface represents the optimal threshold range and resulting best values.

| Stressed | Healthy | Precision | Recall | F-Score | Acc. |
|---------------------|---------------------|-------------|-------------|-------------|-------------|
| 0.19 to 0.40 | 0.40 to 0.50 | 0.94 | 0.98 | 0.96 | 0.96 |
| 0.19 to 0.30 | 0.30 to 0.50 | 0.65 | 0.99 | 0.76 | 0.82 |
| 0.19 to 0.20 | 0.20 to 0.50 | 0.08 | 1.00 | 0.14 | 0.53 |
| 0.19 to 0.35 | 0.35 to 0.50 | 0.86 | 0.99 | 0.91 | 0.95 |

Table 10. Accuracy assessment using different threshold ranges at Level-3b classification for stressed and healthy regions. Note that each row represents the averaged metrics (Precision, Recall, F-score, and Accuracy) of four LGAs under Level-3b classification. The boldface represents the optimal threshold range and resulting best values.

| Stressed | Healthy | Precision | Recall | F-Score | Acc. |
|---------------------|---------------------|-------------|-------------|-------------|-------------|
| 0.50 to 0.60 | 0.60 to 1.00 | 0.82 | 0.86 | 0.86 | 0.85 |
| 0.50 to 0.65 | 0.65 to 1.00 | 0.83 | 0.76 | 0.79 | 0.78 |
| 0.50 to 0.70 | 0.70 to 1.00 | 0.86 | 0.68 | 0.75 | 0.71 |
| 0.50 to 0.75 | 0.75 to 1.00 | 0.87 | 0.55 | 0.66 | 0.62 |

5.3. Analysis of Threshold Ranges

Through Table 7, we notice that non-vegetation regions mostly fall below a 0.19 NDVI value, whereas vegetation falls above it in the context of Victorian LGAs. This finding supports the existing work [12], assuring that the vegetation region normally has a higher NDVI values compared to non-vegetation regions. Furthermore, while observing Table 8, we notice that the range 0.19 to 0.50 within the vegetation is appropriate for shrub and the range (0.50 to 1.00) is for trees class. This statement supports the fact that, as we go higher in the NDVI ranges, trees basically impart a higher NDVI value than shrubs, which is in line with the existing work [57]. Furthermore, Tables 9 and 10 show that the healthy shrub/trees have higher NDVI values than stressed shrub/trees, which is also in line with the existing work [58]. This NDVI trend justifies that healthy vegetation has a higher amount of chlorophyll than stressed vegetation. Given all of these discussions, we underline that NDVI value ranges could be one of the simple but stronger indicators of the LULC classification at different levels.

5.4. Analysis of Vegetation Distribution

Through chord diagram, Figure 6, we identify that there is an imbalance of vegetation and non-vegetation regions in the City of Melbourne, LGA in the level-1 classification (Figure 6a), which has, as a result, affected both per capita green space (90) and urban green space index ($19.78 + 17.0 + 6.9 = 43.68$ green against 56.3 none-green (Table 12). Furthermore, the majority of vegetation regions covered by shrubs shows that there is still some work that needs to be done to balance both shrub and trees under the vegetation class. Furthermore, a higher portion of stressed shrub than healthy shrub attracts the attention of people to focus towards increasing the number of healthy shrubs. Because of a higher number of healthy trees than their stressed counterparts in candidate LGAs (Figure 6), urban planners could focus on shrub categories for balanced vegetation types.

Table 11. Urban Green Space Index (*UGSI*) and Per Capita Green Space (*PCGS*) calculation of different LGAs of Victoria, Australia. Note that the unit of *PCGS* is m^2/person .

| LGA | Area (km^2) | Population | N-Veg (km^2) | Veg (km^2) | <i>UGSI (%)</i> | | | | <i>PCGS</i> |
|---------------|---------------------------|------------|----------------------------|--------------------------|-----------------|-------|-------|-------|-------------|
| | | | | | None | Low | Med. | High | |
| Alpine | 4787 | 12,814 | 52 | 4735 | 0.01 | 13.53 | 39.66 | 46.80 | 369,518 |
| Ararat | 4208 | 11,845 | 1794 | 2414 | 43.00 | 39.13 | 15.49 | 2.38 | 203,799 |
| Ballarat | 738 | 109,505 | 145 | 593 | 19.63 | 55.06 | 18.67 | 6.64 | 5415 |
| Banyule | 62 | 131,631 | 6 | 56 | 10.03 | 37.98 | 45.66 | 6.33 | 425 |
| Baw Baw | 4023 | 53,396 | 51 | 3972 | 1.27 | 5.22 | 29.55 | 63.96 | 74,388 |
| Bayside | 36 | 106,862 | 5 | 31 | 13.62 | 36.60 | 42.82 | 6.96 | 290 |
| Benalla | 2348 | 14,037 | 932 | 1416 | 39.66 | 27.42 | 24.19 | 8.73 | 100,876 |
| Boroondara | 60 | 183,199 | 6 | 54 | 10.51 | 35.36 | 49.58 | 4.55 | 295 |
| Brimbank | 121 | 209,523 | 23 | 98 | 19.18 | 28.12 | 41.62 | 11.08 | 468 |
| Buloke | 7944 | 6124 | 7779 | 165 | 97.90 | 2.08 | 0.01 | 0.01 | 26,943 |
| Campaspe | 4517 | 37,622 | 2965 | 1552 | 65.62 | 23.21 | 9.70 | 1.47 | 41,252 |
| Cardinia | 1270 | 112,159 | 36 | 1234 | 2.85 | 21.50 | 56.69 | 18.96 | 11,002 |
| Casey | 401 | 353,872 | 39 | 362 | 9.70 | 39.10 | 46.39 | 4.81 | 1023 |
| C. Goldfields | 1533 | 13,186 | 647 | 886 | 42.56 | 31.52 | 25.91 | 0.01 | 67,192 |
| Colac-Otway | 3368 | 21,564 | 111 | 3257 | 3.29 | 31.04 | 20.10 | 45.57 | 151,039 |
| Corangamite | 4403 | 16,020 | 551 | 3852 | 12.52 | 39.51 | 30.43 | 17.54 | 240,449 |
| Darebin | 53 | 164,184 | 12 | 41 | 23.44 | 42.44 | 31.03 | 3.09 | 250 |
| E. Gippsland | 19,640 | 47,316 | 341 | 19,299 | 1.73 | 7.48 | 53.11 | 37.68 | 407,875 |
| Frankston | 128 | 142,643 | 12 | 116 | 9.73 | 22.44 | 48.94 | 18.89 | 813 |
| Gannawarra | 3734 | 10,472 | 2879 | 855 | 77.10 | 18.41 | 4.13 | 0.36 | 81,646 |
| Glen Eira | 38 | 156,511 | 7 | 31 | 18.23 | 50.71 | 28.96 | 2.10 | 198 |
| Glenelg | 6211 | 19,674 | 160 | 6051 | 2.56 | 37.70 | 33.69 | 26.05 | 307,563 |
| Golden Plains | 2703 | 23,722 | 300 | 2403 | 11.09 | 61.59 | 24.36 | 2.96 | 101,298 |
| G. Bendigo | 2999 | 118,093 | 1157 | 1842 | 38.58 | 38.53 | 22.61 | 0.28 | 15,598 |
| G. Dandenong | 127 | 168,201 | 37 | 90 | 29.22 | 43.25 | 25.83 | 1.70 | 535 |
| G. Geelong | 1244 | 258,934 | 282 | 962 | 22.64 | 59.46 | 16.70 | 1.20 | 3715 |

Through three Tables 11–13, we identify that Buloke, which has the least vegetation regions in all three aspects (low, medium, and high), is the poorest green space abundance LGA with respect to its total area. Thus, it is important to increase the green spaces in the LGA to balance with the non-green spaces for its sustainability. Furthermore, we underscore that Melbourne, which is located in the central city area of Melbourne, needs to increase more green spaces in the region to improve *PCGS* compared to other LGAs in Victoria, Australia. Such increment of green spaces in the region not only helps improve attachment of people with the nature but also helps balance the risks engendered by widespread over-urbanization. To this end, we can say that there are several LGAs in Victoria including Buloke (S), which have a lower *UGSI* and *PCGS* metrics and such results impose an alarming situation to maintain the eco-friendly urbanization and healthy lifestyle of urban dwellers.

Shekhar and Aryal [51] calculated *UGSI* and *PCGS* for the Kalaburagi city of Karnataka, India with the high-resolution remote sensing data and object-based approach. Their result shows that the average green space and per capita green space is 21.3% and 25 m^2 , respectively. Furthermore, Wustemann et al. [59] carried out research to calculate the *UGSI* of different cities of Germany. Their result shows that there is a range of *UGSI* from 36 m^2 to 2.5 m^2 , which reveals that there is uneven distribution of green space across different cities. Similarly, Beiranvand et al. [60] conducted a study to see the changes in per capita green space index in Khorramabad city of Iran. Their result reveals that per capita green space index of such city remains 5.27, 4.2, 7.73, and 6.88 square meters in 1956, 1974, 1994 and 2006, respectively. Furthermore, Franco et al. [61] carried out a study to observe the per capita urban green space index in Bogota, Colombia. Their results show that Bogota

has the per capita green space index of 4 m^2 . Recently, Huang et al. [62] conducted a study to find the urban green spaces of 1039 cities of the world using Landsat and Google Earth images. Their result shows that high-income cities have a higher urban green space index than low-income cities in the world. In this study, our result shows the maximum high urban green space index and per capita green space index as 67.62% (Yarra Ranges) and $1,589,430 \text{ m}^2/\text{person}$ (West Wimmera) in Victoria, Australia, respectively. This result suggests the comparatively better urban green space index and per capita green space index in comparison with other cities in the world. While comparing our approach with others, our method exploits the normal NDVI measure at the pixel-level to calculate such measures, which is shown to be prominent in the Australian context.

Table 12. Urban Green Space Index (UGSI) and Per Capita Green Space (PCGS) calculation of different LGAs of Victoria, Australia. Note that the unit of PCGS is m^2/person .

| LGA | Area (km ²) | Population | N-Veg (km ²) | Veg (km ²) | UGSI (%) | | | | PCGS |
|---------------|----------------------------|------------|-----------------------------|---------------------------|----------|-------|-------|-------|---------|
| | | | | | None | Low | Med. | High | |
| G. Shepparton | 2418 | 66,498 | 1441 | 977 | 59.59 | 29.99 | 9.40 | 1.02 | 14,692 |
| Hepburn | 1473 | 15,975 | 272 | 1201 | 18.44 | 31.78 | 32.03 | 17.75 | 75,180 |
| Hindmarsh | 7501 | 5588 | 4714 | 2787 | 62.84 | 37.13 | 0.02 | 0.01 | 498,747 |
| Hobsons Bay | 62 | 97,751 | 19 | 43 | 30.54 | 34.91 | 31.25 | 3.30 | 440 |
| Horsham | 4253 | 19,921 | 2474 | 1779 | 58.17 | 30.17 | 11.53 | 0.13 | 89,303 |
| Hume | 497 | 233,471 | 73 | 314 | 14.68 | 63.32 | 21.14 | 0.86 | 1345 |
| Indigo | 1937 | 16,701 | 536 | 1401 | 27.66 | 34.97 | 29.70 | 7.67 | 83,887 |
| Kingston | 90 | 165,782 | 24 | 66 | 27.30 | 40.87 | 29.13 | 2.70 | 398 |
| Knox | 113 | 164,538 | 14 | 99 | 12.50 | 32.57 | 49.38 | 5.55 | 602 |
| Latrobe | 1418 | 75,561 | 44 | 1374 | 3.11 | 5.00 | 30.38 | 61.51 | 18,184 |
| Loddon | 6699 | 7504 | 4745 | 1954 | 70.82 | 20.79 | 8.11 | 0.28 | 260,394 |
| M. Ranges | 1745 | 50,231 | 121 | 1624 | 6.94 | 55.79 | 25.74 | 11.53 | 32,331 |
| Manningham | 113 | 127,573 | 6 | 107 | 5.15 | 25.96 | 59.84 | 9.05 | 839 |
| Mansfield | 3839 | 9176 | 129 | 3710 | 3.35 | 17.31 | 32.84 | 46.50 | 404,316 |
| Maribyrnong | 30 | 93,448 | 11 | 19 | 34.92 | 34.78 | 25.81 | 4.49 | 203 |
| Maroondah | 61 | 118,558 | 7 | 54 | 11.88 | 28.28 | 49.14 | 10.70 | 455 |
| Melbourne | 37 | 178,955 | 21 | 16 | 56.33 | 19.78 | 17.00 | 6.89 | 89 |
| Melton | 527 | 164,895 | 161 | 366 | 30.51 | 60.73 | 8.36 | 0.40 | 2220 |
| Mildura | 22,042 | 55,777 | 13,432 | 8610 | 60.93 | 38.54 | 0.52 | 0.01 | 154,365 |
| Mitchell | 2859 | 46,082 | 308 | 2551 | 10.76 | 53.77 | 28.27 | 7.20 | 55,358 |
| Moira | 4018 | 29,925 | 2277 | 1741 | 56.67 | 29.34 | 11.81 | 2.18 | 58,179 |
| Monash | 81 | 202,847 | 14 | 67 | 17.35 | 43.65 | 36.75 | 2.25 | 330 |
| Moonee Valley | 43 | 130,294 | 10 | 33 | 23.77 | 53.63 | 21.74 | 0.86 | 253 |
| Moorabool | 2110 | 35,049 | 224 | 1886 | 10.63 | 39.04 | 29.59 | 20.74 | 53,810 |
| Moreland | 51 | 185,767 | 13 | 38 | 25.87 | 51.78 | 20.75 | 1.60 | 205 |
| M. Peninsula | 722 | 167,636 | 24 | 698 | 3.30 | 7.91 | 49.26 | 39.53 | 4164 |
| Mt. Alexander | 1530 | 19,754 | 286 | 1244 | 18.68 | 51.05 | 29.65 | 0.62 | 62,975 |

5.5. Implication of Our Database in Greenprinting

Our database can be used in different domains, such as biodiversity conservation, bushfire modelling, land management, urban planning tasks, agriculture monitoring, water resource management, and, most importantly, greenprinting versus blueprint in developing sustainable urban (green/non-green) infrastructure. The Sentinel-2A dataset and derived products are useful to learn the properties of different objects or regions present on the landscape (Figure 7). For example, the Near infrared (NIR) bands are useful to extract several vegetation information on different hierarchical scale such as landscape and streetscape level in urban settings. The information like reflectance, chlorophyll concentration, etc. will help in identifying the present scenario of green regions and their future prospects. Furthermore, using the classified vegetation maps and demographic data,

we are able to study the Victorian population and their association with urban greenness. With the numbers revealed from Urban Green Space Index (*UGSI*) and Per Capita Green Space (*PCGS*) index, the density of population attached to the green space helps to further develop greenprinting. The spatial analysis units that are compatible to local government areas and corresponding statistics and developed urban green space maps are the key first hand information in developing knowledge for policy makers towards greenprinting.

Table 13. Urban Green Space Index (*UGSI*) and Per Capita Green Space (*PCGS*) calculation of different LGAs of Victoria, Australia. Note that the unit of *PCGS* is m^2/person .

| LGA | Area (km^2) | Population | N-Veg (km^2) | Veg (km^2) | <i>UGSI (%)</i> | | | | PCGS |
|--------------|---------------------------|------------|----------------------------|--------------------------|-----------------|-------|-------|-------|-----------|
| | | | None | Low | Med. | High | | | |
| Moyné | 5476 | 16,953 | 498 | 4978 | 9.08 | 64.88 | 20.68 | 5.36 | 293,635 |
| Murrindindi | 3876 | 14,570 | 125 | 3751 | 3.24 | 31.61 | 33.27 | 31.88 | 257,447 |
| Nillumbik | 431 | 65,094 | 11 | 420 | 2.55 | 25.97 | 59.32 | 12.16 | 6452 |
| N. Grampians | 5723 | 11,402 | 2752 | 2971 | 48.08 | 29.45 | 20.53 | 1.94 | 260,568 |
| Port Phillip | 20 | 115,601 | 8 | 12 | 42.28 | 31.46 | 21.14 | 5.12 | 104 |
| Pyrenees | 3434 | 7472 | 1134 | 2300 | 33.00 | 41.39 | 23.03 | 2.58 | 307,816 |
| Queenscliffe | 8 | 2940 | 1 | 7 | 10.60 | 58.16 | 31.23 | 0.01 | 2381 |
| S. Gippsland | 3257 | 29,914 | 36 | 3221 | 1.09 | 6.60 | 41.07 | 51.24 | 107,675 |
| S. Grampians | 6653 | 16,100 | 821 | 5832 | 12.33 | 60.85 | 23.80 | 3.02 | 362,236 |
| Stonnington | 26 | 117,768 | 6 | 20 | 22.54 | 38.43 | 35.05 | 3.98 | 170 |
| Strathbogie | 3302 | 10,781 | 1437 | 1865 | 43.52 | 39.25 | 16.96 | 0.27 | 172,990 |
| Surf Coast | 1551 | 33,456 | 73 | 1478 | 4.70 | 17.49 | 42.83 | 34.98 | 44,177 |
| Swan Hill | 6095 | 20,649 | 5132 | 963 | 84.20 | 11.59 | 4.20 | 0.01 | 46,637 |
| Towong | 6664 | 6040 | 164 | 6500 | 2.46 | 26.25 | 42.32 | 28.97 | 1,076,159 |
| Wangaratta | 3586 | 29,187 | 939 | 2647 | 26.17 | 24.88 | 33.90 | 15.05 | 90,691 |
| Warrnambool | 120 | 35,181 | 8 | 112 | 6.46 | 54.68 | 29.77 | 9.09 | 3184 |
| Wellington | 10,513 | 44,380 | 609 | 9904 | 6.46 | 26.79 | 48.33 | 18.42 | 223,164 |
| W. Wimmera | 9100 | 3841 | 2995 | 6105 | 32.91 | 48.31 | 17.89 | 0.89 | 1,589,430 |
| Whitehorse | 64 | 178,739 | 8 | 56 | 12.26 | 37.86 | 47.24 | 2.64 | 313 |
| Whittlesea | 487 | 230,238 | 47 | 440 | 9.56 | 51.85 | 27.68 | 10.91 | 1911 |
| Wodonga | 433 | 42,083 | 150 | 283 | 34.58 | 44.04 | 19.98 | 1.40 | 6725 |
| Wyndham | 540 | 270,487 | 173 | 367 | 32.14 | 58.98 | 7.68 | 1.20 | 1357 |
| Yarra | 19 | 101,495 | 9 | 11 | 44.32 | 27.08 | 23.58 | 5.02 | 108 |
| Yarra Ranges | 2466 | 159,462 | 32 | 2434 | 1.31 | 6.29 | 24.78 | 67.62 | 15,264 |
| Yarriambiack | 7320 | 6639 | 6728 | 592 | 91.90 | 8.08 | 0.01 | 0.01 | 89,170 |

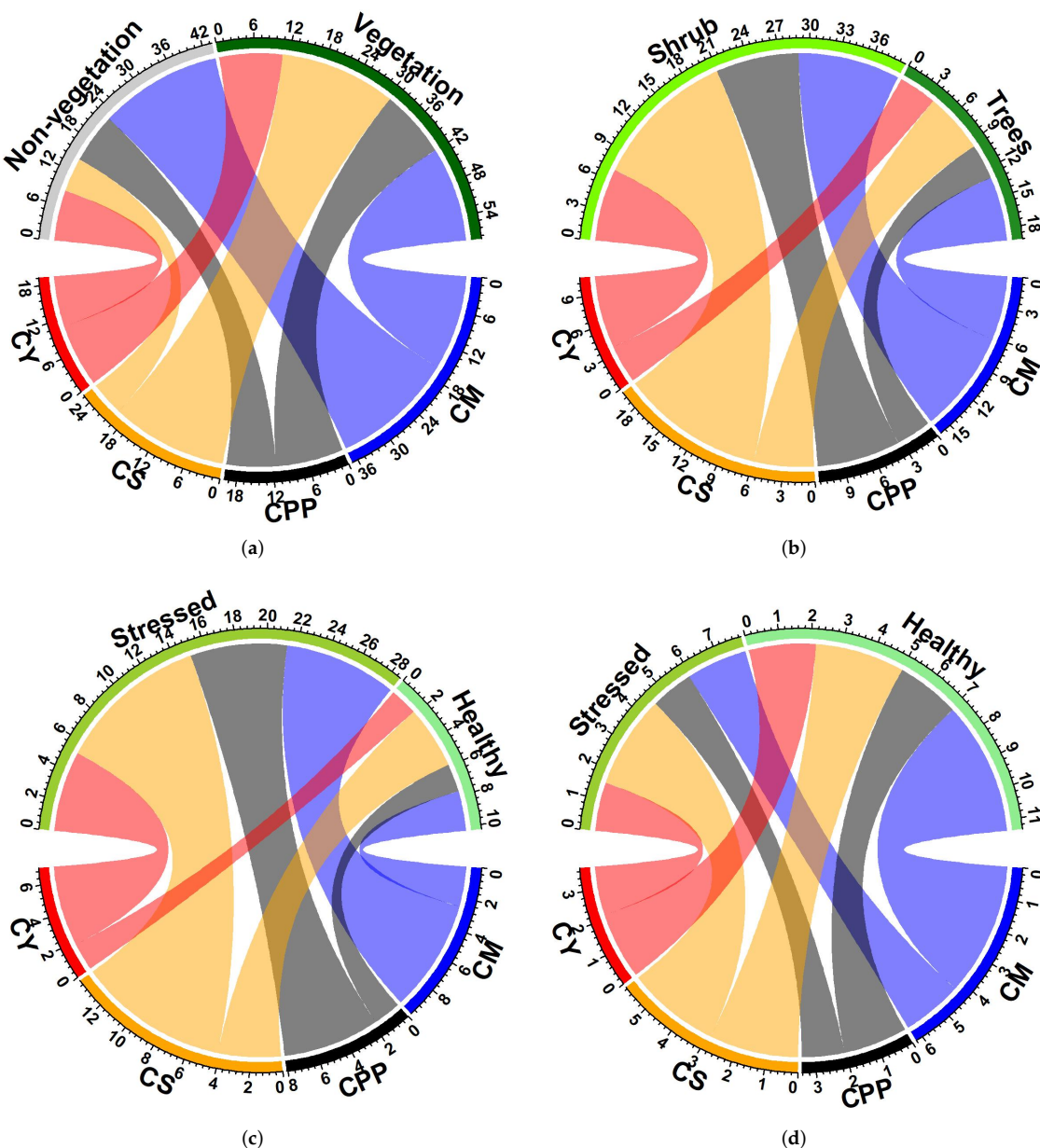


Figure 6. Chord diagram of classification result (in sq. km) of four LGAs of Victoria, Australia, at three levels, namely, (a) Level-1 classification; (b) Level-2 classification; (c) Level-3a classification; and (d) Level-3b classification. Note that CY = City of Yarra; CS = City of Stonnington; CPP = City of Port Phillip; and CM = City of Melbourne.

5.6. Key Contributions of This Study

This study is an applied research with potentials of replicability, reproducibility and interpretability by the researchers as well as practitioners. The applied researchers in the field of land management, urban planning, biodiversity conservation, water run-off modelling and infrastructure design would greatly benefit from the outcome of this research. Furthermore, practitioners working in the various governmental/non-governmental organisation—for example, city councils, planning departments, nature-inspired city planning, land management, and bureau of statistics would benefit not only from urban green space abundance but also from the information on share of green space to per capita. In summary, the key contributions of this research can be framed into the following four points:

1. Integration of publicly available remote sensing image database for each LGA of Victoria (a total of 78 LGAs in our work) based on the Sentinel-2A products. Our database platform is readily useful for different tasks such as systematic urban spatial planning.
2. Hierarchical mapping of urban vegetation into three levels. At the first level (Level-1), we categorise each LGA region into two classes: vegetation and non-vegetation (land). Next, at Level-2, we further categorise the vegetation regions into two sub-classes: shrub and trees. Lastly, at Level-3, both shrub and trees are further categorised into two finer groups: stressed and healthy. The classification maps of three different levels have multiple usability for different stakeholders—for example, biodiversity conservationists, urban planners, bushfire modellers, ecological modellers, and urban agriculture monitoring activities, among many others.
3. Design of experiment based on quantitative iterative optimal approach in ascertaining the NDVI threshold ranges. In doing this, we derive statistical measures such as mean precision, recall, f-score, and accuracy for evaluation purposes. In addition, then, using such metrics, we adopt the best threshold range for each hierarchy.
4. Modelling of association between demography and urban green abundance. In doing this, we compute Urban Green Space Index (*UGSI*) and Per Capita Green Space (*PCGS*) for each Local Government Area (LGA), which will eventually help in sustainability and resilience research of the cities.

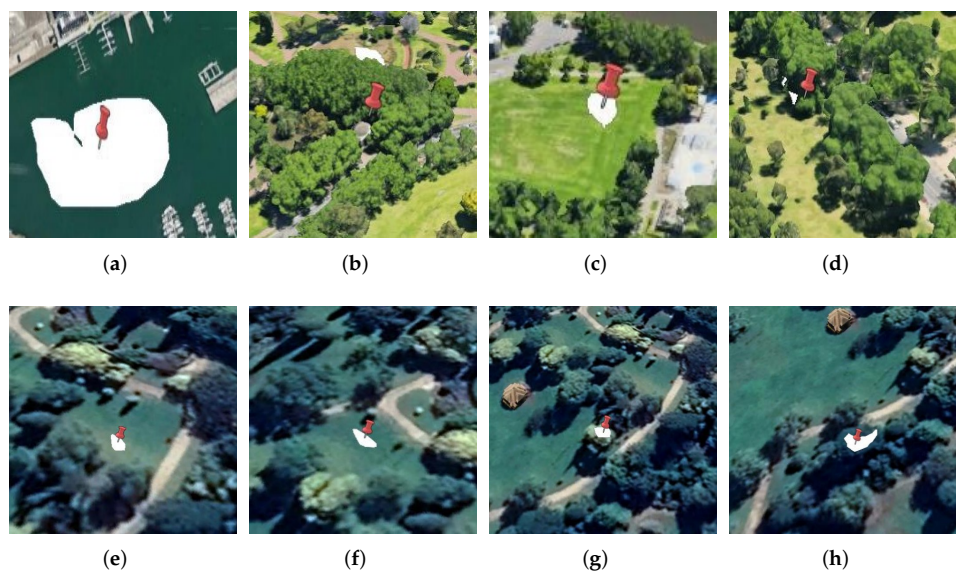


Figure 7. Polygons with place markers ((a) Non-vegetation; (b) Vegetation; (c) Shrub; (d) Trees; (e) Stressed shrub; (f) Healthy shrub; (g) Stressed trees and (h) Healthy trees) that are plotted using Google Earth Engine (GEE) [2] in different regions of City of Melbourne, Victoria, Australia. In our paper, shrub represents grasslands and bushes, whereas trees represent the vegetation except shrub.

5.7. Limitations of This Study and Future Potential

Our method has two main limitations considering the precision of the obtained results and further derivatives. First, simply using NDVI value alone may not provide precise information on landscapes and their coverage. Given that NDVI is the ratio of reflectances, the real world objects having similar reflectances might be classified into the same class/categories. However, we acknowledge that calculating green coverage from NDVI suffices for the purpose of mapping greenness for greenprinting. The derived products from NDVI alone may not be useful in studying vegetation dynamics where methods like radiative transfer modelling having more botanical emphasis would be recommended. Second, NDVI value may be higher for shrubs than trees depending on the crown density and corresponding chlorophyll content alongside healthy and stressed types. Therefore, the classification of regions using NDVI value alone may be erroneous in some cases. To

overcome such problems, we may need to incorporate NDVI value with other widely used spectral indices, such as Enhanced Vegetation Index (EVI), which adopts three bands and imparts other complementary information, namely, canopy structural variations and canopy types based on geometries, etc. NDVI, although an effective vegetation index, is not enough for classification and delineation of land cover types. The thresholds derived in this study may not be useful for other territories or jurisdictions as we have not considered the seasonal variations or phenological changes in this study. To consider these aspects, hyperspectral imagery and periodic 3D-vegetation structure data could greatly improve the resolution and precision of the land cover classification [63].

In the future, we would like to address these limitations and work towards three main directions: (1) use of machine learning and deep learning approaches, both supervised and unsupervised, for more precise classification of urban green space in Victorian LGAs; (2) use of multiple spectral indices in addition to NDVI for the better representation of regions requiring multiple information; and (3) use of machine learning techniques to perform change detection over an extended period of time using time-series products of satellite images in LGAs of Victoria, Australia.

6. Conclusions

In this study, we have developed urban green space map in three different classification levels (Level-1, Level-2, and, Level-3a and Level-3b) for Victoria, Australia using a low cost approach utilizing publicly available Sentinel-2A products and open source platforms Google Earth Engine (GEE) and Geographic Information System software—QGIS. For this, we have tested different NDVI threshold value ranges (e.g., 0.19 to 0.50 for shrub, 0.50 to 1.00 for trees, etc.) in relation to Victoria, Australia, which will be easy to replicate in the future. We relate the urban dwellers population with the urban green space by developing indices on Urban green space and per capita green space in providing first hand information to land managers and policy makers to help increase the greenness of the LGAs. We also prepared a Sentinel-2A dataset of Victorian LGAs, which could be used for other research directions such as crop monitoring, sustainable urban planning, observation of coastal zones, environment monitoring, inland water monitoring, and most importantly on greenprinting. In addition, the combination of our datasets with other kinds of datasets such as weather and non-image datasets could help build the multimodal approach for better classification. Our results suggest that even a simple use of NDVI can produce a green coverage map for the wider application in greenprinting.

Supplementary Materials: The following supporting information can be downloaded at: <https://www.mdpi.com/article/10.3390/land11030351/s1>. The supplementary File S1 contains the following information: (1) A table containing four different threshold ranges at three different levels. (2) Corresponding output maps based on the threshold values as presented in Table above. The supplementary File S2 contains the following information: (1) Sentinel-2A image (RGB) of each LGA of Victoria, Australia. (2) Visual area coverage of each LGA of Victoria, Australia. (3) Classified output images at three different classification levels (Level-1, Level-2, Level-3a, and Level-3b) of each LGA of Victoria, Australia. Here, we have added the larger-sized output maps for three LGAs.

Author Contributions: Conceptualization, J.A. and C.S.; methodology, J.A., C.S. and S.A.; software, C.S.; validation, J.A., C.S. and S.A.; formal analysis, J.A.; investigation, J.A.; resources, J.A.; data curation, C.S.; writing—original draft preparation, J.A. and C.S.; writing—review and editing, J.A., C.S. and S.A.; visualization, J.A. and C.S.; supervision, J.A.; project administration, J.A. All authors have read and agreed to the published version of the manuscript.

Funding: This research received no funding.

Institutional Review Board Statement: Not applicable.

Informed Consent Statement: Not applicable.

Data Availability Statement: Not applicable.

Conflicts of Interest: The authors declare no conflict of interest.

Note

1 We exclude Bass Coast Shire in our work because Copernicus Open Access Hub did not allow us download the Sentinel-2A image.

References

1. Simonetti, E.; Simonetti, D.; Preatoni, D. *Phenology-Based Land Cover Classification Using Landsat 8 Time Series*; European Commission Joint Research Center: Ispra, Italy, 2014.
2. Gorelick, N.; Hancher, M.; Dixon, M.; Ilyushchenko, S.; Thau, D.; Moore, R. Google Earth Engine: Planetary-scale geospatial analysis for everyone. *Remote Sens. Environ.* **2017**, *202*, 18–27. [[CrossRef](#)]
3. Copernicus Open Access Portal. 2020. Available online: <https://scihub.copernicus.eu/> (accessed on 10 September 2020).
4. EO Browser. 2020. Available online: <https://www.sentinel-hub.com/explore/eobrowser/> (accessed on 23 November 2020).
5. Earth Explorer. 2020. Available online: <https://earthexplorer.usgs.gov/> (accessed on 23 November 2020).
6. El-Mezouar, C.; Taleb, N.; Kpalma, K.; Ronsin, J. A high-resolution index for vegetation extraction in IKONOS images. In *Proceedings of the Remote Sensing for Agriculture, Ecosystems, and Hydrology XII, Toulouse, France, 20–22 September 2010*; International Society for Optics and Photonics: Bellingham, WA, USA, 2010; Volume 7824, p. 78242A.
7. Li, F.; Han, L.; Zhu, L.; Huang, Y.; Song, G. Urban Vegetation mapping based on the hj-a ndvi reconstruction. *Int. Arch. Photogramm. Remote Sens. Spat. Inf. Sci.* **2016**, *41*, 867–871. [[CrossRef](#)]
8. Yu, F.; Price, K.; Ellis, J.; Kastens, D. Satellite observations of the seasonal vegetation growth in central asia: 1982–1990. *Photogramm. Eng. Remote Sens.* **2004**, *70*, 461–469. [[CrossRef](#)]
9. Ghaderpour, E.; Ben Abbes, A.; Rhif, M.; Pagiatakis, S.D.; Farah, I.R. Non-stationary and unequally spaced NDVI time series analyses by the LSWAVE software. *Int. J. Remote Sens.* **2020**, *41*, 2374–2390. [[CrossRef](#)]
10. Abdullah, A.Y.M.; Masrur, A.; Adnan, M.S.G.; Baky, M.; Al, A.; Hassan, Q.K.; Dewan, A. Spatio-temporal patterns of land use/land cover change in the heterogeneous coastal region of Bangladesh between 1990 and 2017. *Remote Sens.* **2019**, *11*, 790. [[CrossRef](#)]
11. Kwan, C.; Gribben, D.; Ayhan, B.; Li, J.; Bernabe, S.; Plaza, A. An accurate vegetation and non-vegetation differentiation approach based on land cover classification. *Remote Sens.* **2020**, *12*, 3880. [[CrossRef](#)]
12. Montandon, L.; Small, E. The impact of soil reflectance on the quantification of the green vegetation fraction from NDVI. *Remote Sens. Environ.* **2008**, *112*, 1835–1845. [[CrossRef](#)]
13. Sahebjalal, E.; Dashtekian, K. Analysis of land use-land covers changes using normalized difference vegetation index (NDVI) differencing and classification methods. *Afr. J. Agric. Res.* **2013**, *8*, 4614–4622.
14. Gascon, M.; Cirach, M.; Martínez, D.; Dadvand, P.; Valentín, A.; Nieuwenhuijsen, M. Normalized difference vegetation index (NDVI) as a marker of surrounding greenness in epidemiological studies: The case of Barcelona city. *Urban For. Urban Green.* **2016**, *19*, 88–94. [[CrossRef](#)]
15. Da Silva, V.; Salami, G.; da Silva, M.; Silva, E.; Monteiro Junior, J.; Alba, E. Methodological evaluation of vegetation indexes in land use and land cover (LULC) classification. *Geol. Ecol. Landscapes* **2020**, *4*, 159–169. [[CrossRef](#)]
16. Mensah, A.; Sarfo, D.; Partey, S. Assessment of vegetation dynamics using remote sensing and GIS: A case of Bosomtwe Range Forest Reserve, Ghana. *Egypt. J. Remote Sens. Space Sci.* **2019**, *22*, 145–154.
17. Daryaei, A.; Sohrabi, H.; Atzberger, C.; Immitzer, M. Fine-scale detection of vegetation in semi-arid mountainous areas with focus on riparian landscapes using Sentinel-2 and UAV data. *Comput. Electron. Agric.* **2020**, *177*, 105686. [[CrossRef](#)]
18. Abutaleb, K.; Mudede, M.; Nkongolo, N.; Newete, S. Estimating urban greenness index using remote sensing data: A case study of an affluent vs poor suburbs in the city of Johannesburg. *Egypt. J. Remote Sens. Space Sci.* **2020**, *24*, 343–351. [[CrossRef](#)]
19. Cai, Y.; Zhang, M.; Lin, H. Estimating the urban fractional vegetation cover using an object-based mixture analysis method and Sentinel-2 MSI imagery. *IEEE J. Sel. Top. Appl. Earth Obs. Remote Sens.* **2020**, *13*, 341–350. [[CrossRef](#)]
20. Zhang, T.; Su, J.; Liu, C.; Chen, W.H.; Liu, H.; Liu, G. Band selection in Sentinel-2 satellite for agriculture applications. In *Proceedings of the 23rd International Conference on Automation and Computing (ICAC)*, Huddersfield, UK, 7–8 September 2017; pp. 1–6.
21. Liu, Y.; Gong, W.; Hu, X.; Gong, J. Forest type identification with random forest using Sentinel-1A, Sentinel-2A, multi-temporal Landsat-8 and DEM data. *Remote Sens.* **2018**, *10*, 946. [[CrossRef](#)]
22. Vasilakos, C.; Kavroudakis, D.; Georganta, A. Machine learning classification ensemble of multi-temporal sentinel-2 images: The case of a mixed mediterranean ecosystem. *Remote Sens.* **2020**, *12*, 2005. [[CrossRef](#)]
23. Wei, M.; Qiao, B.; Zhao, J.; Zuo, X. The area extraction of winter wheat in mixed planting area based on Sentinel-2 a remote sensing satellite images. *Int. J. Parallel, Emergent Distrib. Syst.* **2020**, *35*, 297–308. [[CrossRef](#)]
24. Ghorbanzadeh, O.; Blaschke, T.; Gholamnia, K.; Meena, S.; Tiede, D.; Aryal, J. Evaluation of different machine learning methods and deep-learning convolutional neural networks for landslide detection. *Remote Sens.* **2019**, *11*, 196. [[CrossRef](#)]
25. Timilsina, S.; Aryal, J.; Kirkpatrick, J. Mapping Urban Tree Cover Changes Using Object-Based Convolution Neural Network (OB-CNN). *Remote Sens.* **2020**, *12*, 3017. [[CrossRef](#)]
26. Li, W.; Fu, H.; Yu, L.; Gong, P.; Feng, D.; Li, C.; Clinton, N. Stacked Autoencoder-based deep learning for remote-sensing image classification: A case study of African land-cover mapping. *Int. J. Remote Sens.* **2016**, *37*, 5632–5646. [[CrossRef](#)]
27. Liang, P.; Shi, W.; Zhang, X. Remote sensing image classification based on stacked denoising autoencoder. *Remote Sens.* **2018**, *10*, 16. [[CrossRef](#)]

28. Tong, X.Y.; Xia, G.S.; Lu, Q.; Shen, H.; Li, S.; You, S.; Zhang, L. Land-cover classification with high-resolution remote sensing images using transferable deep models. *Remote Sens. Environ.* **2020**, *237*, 111322. [[CrossRef](#)]
29. Bramhe, V.; Ghosh, S.; Garg, P. Extraction of built-up areas using convolutional neural networks and transfer learning from sentinel-2 satellite images. *Int. Arch. Photogramm. Remote Sens. Spat. Inf. Sci.* **2018**, *42*, 79–85. [[CrossRef](#)]
30. Luo, X.; Tong, X.; Hu, Z.; Wu, G. Improving urban land cover/use mapping by integrating a hybrid convolutional neural network and an automatic training sample expanding strategy. *Remote Sens.* **2020**, *12*, 2292. [[CrossRef](#)]
31. Kocev, D.; Džeroski, S.; White, M.; Newell, G.; Griffioen, P. Using single-and multi-target regression trees and ensembles to model a compound index of vegetation condition. *Ecol. Model.* **2009**, *220*, 1159–1168. [[CrossRef](#)]
32. Sheffield, K.; Morse-McNabb, E.; Clark, R.; Robson, S.; Lewis, H. Mapping dominant annual land cover from 2009 to 2013 across Victoria, Australia using satellite imagery. *Sci. Data* **2015**, *2*, 1–15. [[CrossRef](#)]
33. QGIS Development Team. *QGIS Geographic Information System*; Open Source Geospatial Foundation: Beaverton, OR, USA, 2009.
34. Breiman, L. Random forests. *Mach. Learn.* **2001**, *45*, 5–32. [[CrossRef](#)]
35. Cristianini, N.; Shawe-Taylor, J. *An Introduction to Support Vector Machines and Other Kernel-based Learning Methods*; Cambridge University Press: Cambridge, UK, 2000.
36. Dempster, A.; Laird, N.; Rubin, D. Maximum likelihood from incomplete data via the EM algorithm. *J. R. Stat. Soc. Ser. (Methodol.)* **1977**, *39*, 1–22.
37. Abdi, A. Land cover and land use classification performance of machine learning algorithms in a boreal landscape using Sentinel-2 data. *Giscience Remote Sens.* **2020**, *57*, 1–20. [[CrossRef](#)]
38. Chen, T.; Guestrin, C. Xgboost: A scalable tree boosting system. In Proceedings of the 22nd ACM Sigkdd International Conference on Knowledge Discovery and Data Mining, San Francisco, CA, USA, 13–17 August 2016; pp. 785–794.
39. He, K.; Zhang, X.; Ren, S.; Sun, J. Deep residual learning for image recognition. In Proceedings of the IEEE Conference Computer vision and Pattern Recognition (CVPR), Las Vegas, NV, USA, 27–30 June 2016; pp. 770–778.
40. Simonyan, K.; Zisserman, A. Very deep convolutional networks for large-scale image recognition. *arXiv* **2014**, arXiv:1409.1556.
41. Szegedy, C.; Vanhoucke, V.; Ioffe, S.; Shlens, J.; Wojna, Z. Rethinking the inception architecture for computer vision. In Proceedings of the IEEE Conference on Computer Vision and Pattern Recognition (CVPR), Las Vegas, NV, USA, 27–30 June 2016; pp. 2818–2826.
42. Victorian LGA. 2020. <https://discover.data.vic.gov.au/dataset/lga/> (accessed on 10 September 2020).
43. Victorian Vegetation. 2020. Available online: <http://www.vicveg.net.au/vvPlantNote2.aspx/> (accessed on 23 November 2020).
44. Victorian Vegetation Communities. 2020. Available online: <https://www.necma.vic.gov.au/Solutions/Plants-Animals/Native-Plants-Animals/Vegetation-communities-revegetation/> (accessed on 23 November 2020).
45. Victorian Climate Temperature. 2020. Available online: <http://vro.agriculture.vic.gov.au/dpi/vro/vrosite.nsf/pages/climate-temperature/> (accessed on 23 November 2020).
46. Szantoi, Z.; Strobl, P. Copernicus Sentinel-2 Calibration and Validation. *Eur. J. Remote Sens.* **2019**, *52*, 253–255. [[CrossRef](#)]
47. Sentinel-2A Products. 2020. Available online: <https://sentinel.esa.int/web/sentinel/user-guides/sentinel-2-msi/product-types/> (accessed on 22 November 2020).
48. Sentinel-2A Guidelines. 2020. Available online: <https://sentinel.esa.int/web/sentinel/technical-guides/sentinel-2-msi/level-2a/algorithms/> (accessed on 22 November 2020).
49. Sentinel-2A Processing Levels. 2020. Available online: <https://sentinel.esa.int/web/sentinel/user-guides/sentinel-2-msi/processing-levels/level-2/> (accessed on 11 July 2020).
50. Bannari, A.; Morin, D.; Bonn, F.; Huete, A. A review of vegetation indices. *Remote Sens. Rev.* **1995**, *13*, 95–120. [[CrossRef](#)]
51. Shekhar, S.; Aryal, J. Role of geospatial technology in understanding urban green space of Kalaburagi city for sustainable planning. *Urban For. Urban Green.* **2019**, *46*, 126450. [[CrossRef](#)]
52. Australian Bureau of Statistics. 2020. Available online: <https://itt.abs.gov.au/itt/r.jsp?databyregion/> (accessed on 3 December 2020).
53. R Core Team. *R: A Language and Environment for Statistical Computing*; R Foundation for Statistical Computing: Vienna, Austria, 2013.
54. Ranghetti, L.; Busetto, L. sen2r: Find, Download and Process Sentinel-2 Data. 2019. R Package Version 1.1.0. Available online: <https://sen2r.ranghetti.info/> (accessed on 3 December 2020).
55. Hashim, H.; Abd Latif, Z.; Adnan, N. Urban vegetation classification with NDVI thresold value method with very high resolution (VHR) PLEIADES Imagery. *Int. Arch. Photogramm. Remote Sens. Spat. Inf. Sci.* **2019**, *42*, 237–240. [[CrossRef](#)]
56. Aburas, M.; Abdullah, S.; Ramli, M.; Ash'aari, Z. Measuring land cover change in Seremban, Malaysia using NDVI index. *Procedia Environ. Sci.* **2015**, *30*, 238–243. [[CrossRef](#)]
57. Zaitunah, A.; Samsuri, A.; Safitri, R. Normalized difference vegetation index (ndvi) analysis for land cover types using landsat 8 oli in besitang watershed, Indonesia. In Proceedings of the IOP Conference Series: Earth and Environmental Science, Banda Aceh, Indonesia, 26–27 September 2018; Volume 126, pp. 1–9.
58. Gessesse, A.A.; Melesse, A.M. Temporal relationships between time series CHIRPS-rainfall estimation and eMODIS-NDVI satellite images in Amhara Region, Ethiopia. In *Extreme Hydrology and Climate Variability*; Elsevier: Amsterdam, The Netherlands, 2019; pp. 81–92.

-
59. Wüstemann, H.; Kalisch, D. *Towards a National Indicator for Urban Green Space Provision and Environmental Inequalities in Germany: Method and Findings*; Technical Report, SFB 649 Discussion Paper; Technische Universität Berlin: Berlin, Germany, 2016.
60. Beiranvand, A.; Bonyad, A.E.; Sousani, J. Evaluation of changes in per capita green space through remote sensing data. *Int. J. Adv. Biol. Biomed. Res.* **2013**, *1*, 321–330.
61. Franco Gantiva, J.A.; Páez, D.; Rajabifard, A. Methodological Proposal for Measuring and Predicting Urban Green Space Per Capita in a Land-Use Cover Change Model: Case Study in Bogotá, Colombia. Master’s Thesis, Uniandes, Bogota, Colombia, 2018.
62. Huang, C.; Yang, J.; Clinton, N.; Yu, L.; Huang, H.; Dronova, I.; Jin, J. Mapping the maximum extents of urban green spaces in 1039 cities using dense satellite images. *Environ. Res. Lett.* **2021**, *16*, 064072. [[CrossRef](#)]
63. Kuras, A.; Brell, M.; Rizzi, J.; Burud, I. Hyperspectral and Lidar Data Applied to the Urban Land Cover Machine Learning and Neural-Network-Based Classification: A Review. *Remote Sens.* **2021**, *13*, 3393. [[CrossRef](#)]